Production of the ω meson in the $pd \to {}^3\mathrm{He}\,\omega$ reaction at 1450 MeV and 1360 MeV

K. Schönning,[1] Chr. Bargholtz,[2] M. Bashkanov,[3] M. Berłowski,[4] D. Bogoslawsky,[5] H. Calén,[1] H. Clement,[3] L. Demirörs,[6] C. Ekström,[7] K. Fransson,[1] L. Gerén,[2] L. Gustafsson,[1] B. Höistad,[1] G. Ivanov,[5] M. Jacewicz,[1] E. Jiganov,[5] T. Johansson,[1] S. Keleta,[1] O. Khakimova,[3] K. P. Khemchandani,[8,9] F. Kren,[3] S. Kullander,[1] A. Kupść,[1] A. Kuzmin,[10] K. Lindberg,[2] P. Marciniewski,[1] B. Morosov,[5] W. Oelert,[11] C. Pauly,[6] H. Petrén,[1] Y. Petukhov,[5] A. Povtorejko,[5] R. J. M. Y. Ruber,[1] W. Scobel,[6] R. Shafigullin,[12] B. Shwartz,[10] T. Skorodko,[3] V. Sopov,[13] J. Stepaniak,[4] P.-E. Tegnér,[2] P. Thörngren Engblom,[1] V. Tikhomirov,[5] A. Turowiecki,[14] G. J. Wagner,[3] C. Wilkin,[15] M. Wolke,[11] J. Zabierowski,[4] I. Zartova,[2] and J. Złomańczuk[1]

(CELSIUS/WASA Collaboration)

[1]*Department of Physics and Astronomy, Uppsala University, Uppsala, Sweden*

[2]*Department of Physics, Stockholm University, Stockholm, Sweden*

[3]*Physikalisches Institut der Universität Tübingen, Tübingen, Germany*

[4]*Sołtan Institute of Nuclear Studies, Warsaw and Lodz, Poland*

[5]*Joint Institute for Nuclear Research, Dubna, Russia*

[6]*Institut für Experimentalphysik, Universität Hamburg, Hamburg, Germany*

[7]*The Svedberg Laboratory, Uppsala, Sweden*

[8]*Departamento de Física Teórica and IFIC, Centro Mixto Universidad de Valencia-CSIC, Institutos de Investigación de Paterna, Aptd. 22085, E-46071 Valencia, Spain*

[9]*Centro de Física Computacional, Departamento de Física, Universidade de Coimbra, P-3004-516 Coimbra, Portugal*

[10]*Budker Institute of Nuclear Physics, Novosibirsk, Russia*

[11]*Institut für Kernphysik, Forschungszentrum Jülich, Germany*

[12]*Moscow Engineering Physics Institute, Moscow, Russia*

[13]*Institute of Theoretical and Experimental Physics, Moscow, Russia*

[14]*Institute of Experimental Physics, Warsaw, Poland*

[15]*Physics and Astronomy Department, UCL, London, United Kingdom*

(Received 5 February 2009; published 28 April 2009)

The production of ω mesons in the $pd \to {}^3\mathrm{He}\,\omega$ reaction has been studied at two energies near the kinematic threshold, $T_p = 1450$ MeV and $T_p = 1360$ MeV. The differential cross section was measured as a function of the ω c.m. angle at both energies over the whole angular range. Whereas the results at 1360 MeV are consistent with isotropy, strong rises are observed near both the forward and backward directions at 1450 MeV. Calculations made using a two-step model with an intermediate pion fail to reproduce the shapes of the measured angular distributions and also underestimate the total cross sections.

DOI: 10.1103/PhysRevC.79.044002 PACS number(s): 14.40.Cs, 25.40.Ve

I. INTRODUCTION

Extensive studies of ω production in the $\pi^- p \to n\,\omega$ reaction were carried out in the 1970s at the NIMROD synchrotron from the kinematic threshold up to ω c.m. momenta of $p^*_\omega = 260$ MeV/c [1–3]. Though the differential cross sections were found to be isotropic, the data also showed a remarkable suppression of the ω production amplitude near the threshold [2,3]. In the work of Binnie *et al.* [1], where $\pi^- p \to n\,\eta'$, $\pi^- p \to n\,\phi$, and $\pi^- p \to n\,\eta$ were studied with the same apparatus, no similar effects were found in the η' and ϕ cases and a threshold enhancement, rather than a suppression, was observed for the η. First, a final state interaction (FSI) effect, where one of the pions from the ω decay scatters off the recoiling neutron, was suggested as a possible explanation for the ω threshold suppression [1]. This explanation was however tested and abandoned in Keyne *et al.* [2], where an alternative explanation were advanced in terms of a combination of s- and p-wave resonances.

The data available for ω production in $pd \to {}^3\mathrm{He}\,\omega$ are rather scarce. The reaction was first studied near its kinematic threshold at SATURNE [4]. The differential cross section at $T_p = 1450$ MeV($p^*_\omega = 280$ MeV/c) measured in the forward and backward regions with the SPESIII spectrometer [5] showed clear anisotropy in θ^*_ω, with strong peaking at extreme angles. This is in contrast to the angular distributions observed in $\pi^- p \to n\,\omega$, which remain flat up to at least $p^*_\omega \approx 200$ MeV/c [3].

Wurzinger *et al.* measured the $pd \to {}^3\mathrm{He}\,\omega$ cross section at $\theta^*_\omega = 180^\circ$ as a function of energy using the SPESIV spectrometer at SATURNE [6] and found a suppression in the production amplitude near threshold similar to the one observed in the $\pi^- p \to n\omega$ reaction [1–3]. These authors also described their data in terms of the FSI hypothesis. However, the correctness of this interpretation has been questioned for both reactions in Refs. [7,8], where effects associated with the ω width have been stressed.

The production of heavy mesons in pd collisions has been studied theoretically in a two-step model [9–16], which first involves the production of a light meson in the interaction between the incident and one of the target nucleons. In the second step, the light meson interacts with the other target nucleon to create the observed heavy meson. This procedure allows the large momentum transfer to be shared between the nucleons. The predictions of this model have been evaluated for the

specific $pd \rightarrow {}^3\mathrm{He}\,\omega$ reaction [14], but only at the backward angles where data existed [6], and no previous attempts have been made to calculate the full angular distribution.

In this paper, the results of the measurements of ω production in the $pd \rightarrow {}^3\mathrm{He}\,\omega$ reaction by the CELSIUS/WASA collaboration are presented at two different beam kinetic energies, $T_p = 1450$ MeV and $T_p = 1360$ MeV. These correspond, respectively, to ω c.m. momenta of $p^*_\omega = 280$ MeV/c and $p^*_\omega = 144$ MeV/c, i.e., excess energies of 63 MeV and 17 MeV. We have previously reported data on the angular distribution of the ω decay plane that show that the ω is produced largely unpolarized [17], which is in stark contrast to the almost complete polarization of the ϕ from the analogous $pd \rightarrow {}^3\mathrm{He}\,\phi$ reaction [18]. We now provide the corresponding results on the differential cross sections that have been measured over the full angular range. These new data constitute an important input to the intriguing question of how heavy mesons are produced in few-body collisions and, in particular, whether the reaction can be usefully viewed as a sequential two-step process.

The outline of this paper is as follows. We start by introducing the WASA detector before going through the analysis in some detail. This involves principally the ^{3}He identification, event selection, background, and normalization procedure. After describing the acceptance corrections, we show our results and compare them to calculations that have been performed in terms of a two-step model.

II. THE CELSIUS/WASA EXPERIMENT

The measurements of the $pd \rightarrow {}^3\mathrm{He}\,\omega$ reaction were carried out at the The Svedberg Laboratory in Uppsala, Sweden, using the WASA detector [19] which, until June 2005, was an integral part of the CELSIUS storage ring. A deuterium pellet target [20,21] was used in combination with a proton beam. The ^{3}He were detected in the WASA forward detector (FD), which covers laboratory polar angles from 3° to 18° with respect to the beam direction. The forward detector consists of a sector-like window counter (FWC) for triggering, a proportional chamber (FPC) for precise angular information, a trigger hodoscope (FTH) for triggering and off-line particle identification, a range hodoscope (FRH) for energy measurements, particle identification and triggering, an intermediate hodoscope (FRI) for improved track reconstruction and neutron detection and finally a veto hodoscope (FVH) for triggering. All FD elements, except the FPC, are made of plastic scintillators.

Mesons and their decay products are detected mainly in the central detector (CD), which consists of the plastic scintillating barrel (PSB), the mini drift chamber (MDC), and the central scintillating electromagnetic calorimeter (SEC) that is made of CsI crystals. Charged particles, such as pions from ω decay, are distinguished from neutral particles by their signals in the PSB, which also provides angular determination from 24° to 159°. The momenta of charged particles are estimated by tracking in a magnetic field from the SuperConducting Solenoid (SCS) using information from the MDC. The SEC measures angles and energies of photons from meson decays in the polar angle range from 20° to 169°. A schematic overview of the CELSIUS/WASA detector setup is shown in Fig. 1.

A special trigger was developed to select ^{3}He events, which are characterized by one high-energy-deposit hit in the FWC and one hit that overlaps in the azimuthal angle in one of the consecutive detectors [22].

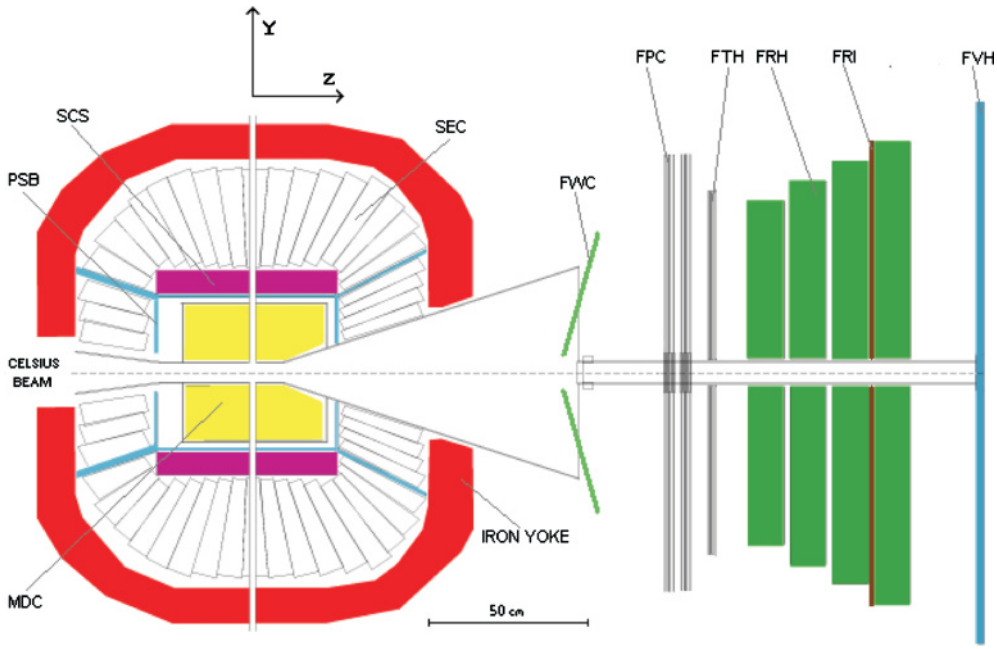

FIG. 1. (Color online) Side view of the CELSIUS/WASA detector setup. The central detector built around the interaction point (to the left) is surrounded by an iron yoke. The layers of the forward detector are shown in the right-hand side. The CELSIUS beam pipe runs horizontally and the target pellets are injected through the vertical pipe. The abbreviations in the figure are explained in the text.

III. ANALYSIS

A. ^{3}He identification

The ^{3}He ions are identified in the FD by the $\Delta E - E$ method. For this the scintillation light output in the detector layer where the particle stops is compared to that in the preceding layer. The particles then show up in different bands, as illustrated in Fig. 2, where the uppermost one represents the ^{3}He. For these candidates the scintillation light output is converted to energy deposit, taking into account the light quenching [23]. This allows the corresponding range to be estimated, which is added to the amount of material traversed by the particle in the preceding detector layers to give the total range. Energy-range tables then allow the initial kinetic energy to be estimated. The expected light output in all the detector layers traversed is calculated and compared to the measured one by evaluating the χ^2, according to

$$\chi^2 = \sum_{i=1}^{N} \left(\Delta L_i^m - \Delta L_i^c\right)^2 / \sigma_i^2 , \qquad (1)$$

where i is the layer number, N the number of layers traversed, ΔL_i^m the measured light output, ΔL_i^c the calculated light output, and σ_i the light output uncertainty in a given layer. The particle is then considered to be properly identified if the calculated χ^2 does not exceed $\chi^2_{\max} = 6.0$. For more details, see Ref. [24].

B. Event selection

In this work, we focus primarily on the $\omega \to \pi^0\pi^+\pi^-$ decay channel because the large branching ratio (BR = 89.1%) gives the high statistics required for the extraction of angular distributions. However, a parallel analysis of the $\omega \to \pi^0\gamma$ decay channel (BR = 8.7%) is a valuable tool for checking that cut efficiencies and other experimental biases are under control.

1. $pd \to {}^3He\,\omega, \omega \to \pi^0\pi^+\pi^-$ events

To select $\omega \to \pi^0\pi^+\pi^-$ events, we require the ^{3}He ion to be measured in the FD with well defined energy and angle, which means that the ^{3}He has to stop within the FRH. The geometrical acceptance of the FD is 95% at 1450 MeV and 78% at 1360 MeV. The main event loss is due to the ^{3}He emitted at small angles that escape down the beam pipe. The detection efficiency of the FD is further reduced by nuclear interactions in the detector material. The efficiency of detecting a ^{3}He from $pd \to {}^3\mathrm{He}\,\omega$ in the FD, as deduced from Monte Carlo simulations including geometry and detector material responses, is 61% and 54% at 1450 and 1360 MeV, respectively.

In addition to the ^{3}He selection, at least two photons are required in the SEC. Furthermore, one photon pair must have an invariant mass that does not differ from that of the π^0 by more than 45 MeV/c^2, and the missing mass of the $^3\mathrm{He}\,\pi^0$ system must be larger than 250 MeV/c^2, i.e., twice the pion mass, after taking the resolution into account. Finally, two or more hits are needed in the PSB and the total energy deposit in the SEC must not exceed 900 MeV. This rejects candidates with photon signals from accidental events.

These constraints give an overall acceptance of 35% at 1450 MeV and 34% at 1360 MeV. The differential acceptance is shown in Fig. 3 for the two energies as a function of $\cos\theta^*_\omega$.

2. $pd \to {}^3He\,\omega, \omega \to \pi^0\gamma$ events

All final state particles, i.e., the ^{3}He and three photons, can be measured with high acceptance in the $\omega \to \pi^0\gamma$ case. Each event is fully reconstructed, which ensures that the kinematical constraints are fulfilled. Though this leads to a cleaner sample than the three-pion channel, the low branching ratio (BR = 8.7%) yields statistics that are insufficient to provide angular distributions.

Having identified a ^{3}He and three photons, we demand that one photon pair has an invariant mass close to that of

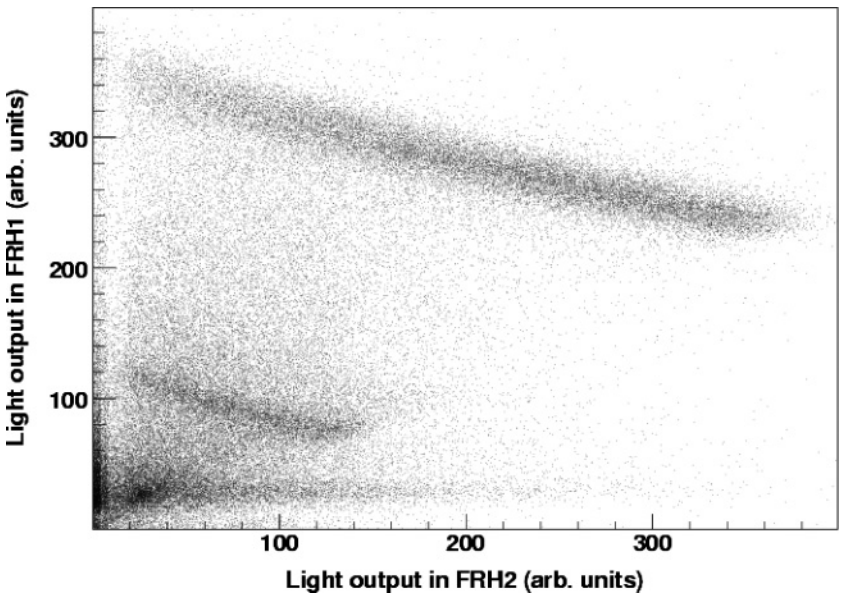

FIG. 2. The scintillation light output in the first layer of the FRH versus the light output in the second layer for particles stopping in the second layer. The data are collected with the ^{3}He trigger which gives a pronounced band with high energy deposit that corresponds to ^{3}He ions. Below is a band of stopping protons and an intense spot at the bottom left corresponds to minimum ionizing particles, coming from events that accidentally fired the ^{3}He trigger. A very weak region corresponding to stopped deuterons might be seen above the proton band.

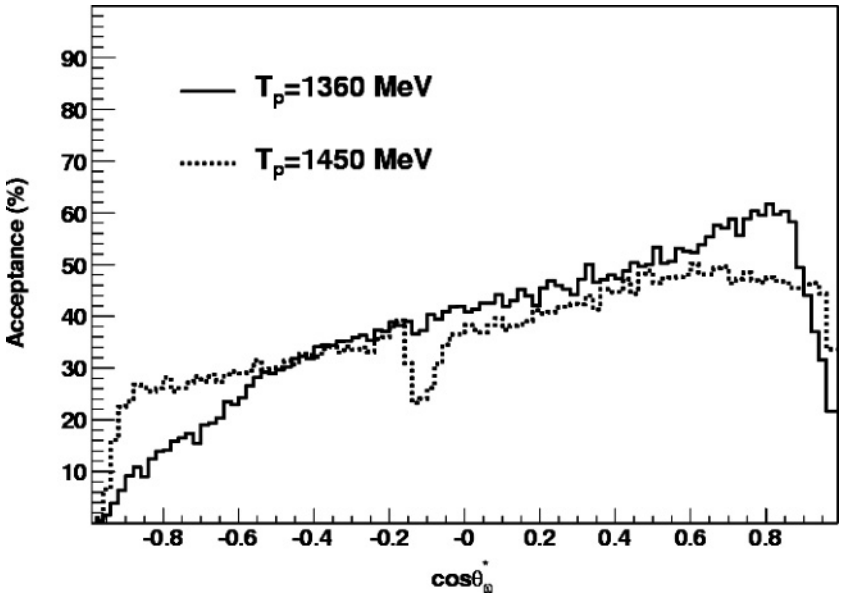

FIG. 3. The acceptance for the $pd \to {}^3\mathrm{He}\,\omega$, $\omega \to \pi^+\pi^-\pi^0$ reaction as a function of $\cos\theta^*_\omega$ at 1360 MeV (solid line) and 1450 MeV (broken line) after applying the cuts explained in the text. The dip in the 1450 MeV distribution corresponds to the ^{3}He that stop between the first and second layer of the FRH.

the π^0, $|IM(\gamma\gamma) - m_{\pi^0}| < 45$ MeV/c^2, and that the invariant mass of all three photons is larger than 600 MeV/c^2. The missing-mass-squared of the ^{3}He $\gamma\gamma\gamma$ system must not exceed $(100)^2$ MeV$^2/c^4$. We also require that the difference between the directions of the missing momentum of the ^{3}He and that of the 3γ system be smaller than 20°. As in the three-pion case, a limit is placed on the total energy deposit in the SEC, which may not exceed 1200 MeV. Finally, a coplanarity cut is applied: $160^\circ < |\phi_{\mathrm{lab}}(^3\mathrm{He}) - \phi_{\mathrm{lab}}(3\gamma)| < 200^\circ$. These constraints reject very effectively the contribution from accidentals and events originating far from the target region. They give acceptances of 19% and 18% at 1450 MeV and 1360 MeV, respectively.

C. Backgrounds

In the three-pion case, the principal background is direct pion production, i.e., $pd \to {}^3\mathrm{He}\,\pi^0\pi^+\pi^-$, which has exactly the same signature as ω production. The acceptance for this background, assuming phase space production, is 31% at 1450 MeV and 35% at 1360 MeV.

Both ω and direct 3π events are produced mainly through the interaction of the beam with the pellet target. However, such reactions can also occur through interactions of the beam with the rest gas, the beam halo with the rest gas, and the beam halo with the beam pipe. Rest gas is produced when the pellets are vaporized by the beam [25] or when the pellets are not properly captured in the pellet beam dump. In the present work, we found that around 30% of the data were not produced from the region of the pellet target. This is in line with the figures obtained from a recent measurement of the $pd \to {}^3\mathrm{He}\,\eta$ reaction at $T_p = 893$ MeV [26]. The vaporization of the pellet is expected to be higher at lower energies [25], but the amount of rest gas also depends upon other time-dependent experimental conditions, such as the beam-target overlap, the efficiency of the vacuum pumps, and the performance of the pellet dump. Since the energy reconstruction procedure assumes that all particles come from a well defined interaction point, the measured energy and momentum of particles produced far from the pellet target will have larger uncertainties and thus degrade the missing-mass resolution. However, the width of the ω peak agrees well with Monte Carlo simulations for a well defined interaction point, which means that most events come either from the target or from the close vicinity. The latter can be treated as good events that do not significantly affect the quality of the data sample.

Monte Carlo simulations show that other channels, such as $pd \to {}^3\mathrm{He}\,\pi^+\pi^-$, $pd \to {}^3\mathrm{He}\,\pi^0\pi^0$, and $pd \to {}^3\mathrm{He}\,\pi^0\pi^0\pi^+\pi^-$, give negligible contributions to the background and will be ignored.

The main background channel in the $\pi^0\gamma$ sample comes from the $pd \to {}^3\mathrm{He}\,\pi^0\pi^0$ reaction, where one of the photons escapes detection. Assuming phase space production, about 1.8% of the $2\pi^0$ events survive the cuts optimized for $\pi^0\gamma$ selection at 1450 MeV and 1.4% at 1360 MeV. Although these are tiny fractions, the two-pion production cross section is large and the $\omega \to \pi^0\gamma$ branching ratio small. Hence it is expected that the numbers of events surviving the cuts should be of the same order of magnitude for the signal and background.

Interactions between the beam halo and the beam pipe, as well as chance coincidences, may also contribute to the background. However, we show in Sec. IV that they only do so to a very limited extent.

D. Normalization

The luminosity depends on the beam intensity and the pellet rate, which are monitored and recorded during the data taking. However, the luminosity also depends on the overlap between the beam and target, which cannot be measured directly. It is also not constant during a run or even over a cycle of data taking. Furthermore, as previously mentioned, as many as

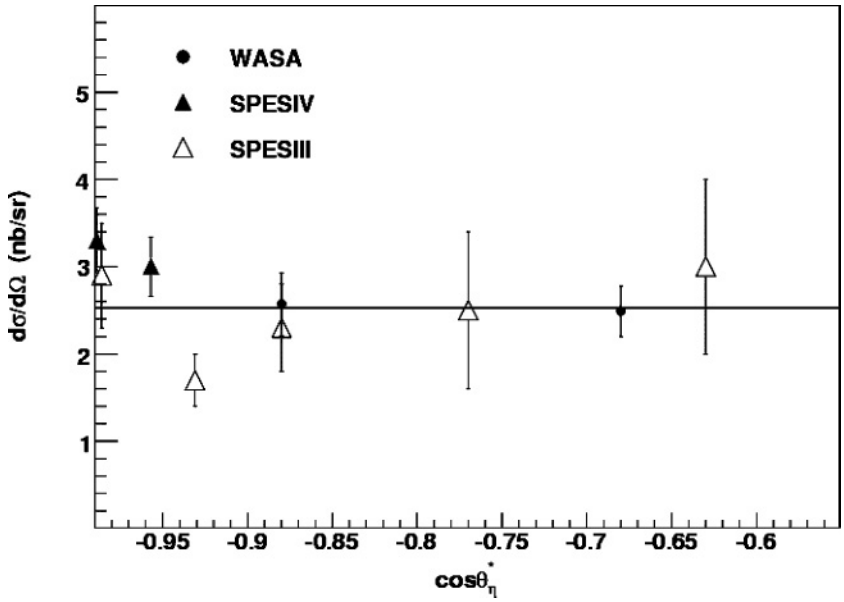

FIG. 4. Differential cross section data for the $pd \to {}^3\mathrm{He}\,\eta$ process at 1450 MeV, which has been used for the evaluation of the luminosity. The filled and unfilled triangles show data from SPESIV [27] and SPESIII [5], respectively. The line is a constant fitted to both sets of data points. The filled circles represent the WASA data after normalization.

30% of the events may result from interactions away from the target. This means that the luminosity must be evaluated by normalizing the number of events of some subsidiary reaction to a well known cross section. Quasielastic pp scattering might be a good choice because the cross section is well known and large statistics are available. However, these data were collected with a different trigger from the ^{3}He events and the relative trigger efficiency is not known with sufficient precision. It is therefore preferable to use a reaction with a ^{3}He in the final state, where the trigger was the same as for $pd \to {}^3\mathrm{He}\,\omega$.

The differential cross section for the $pd \to {}^3\mathrm{He}\,\eta$ reaction was measured at a few very backward angles with the SPESIV spectrometer at 1450, 1350, and 1250 MeV [27]. It was also measured over a larger angular range at 1450 MeV with the SPESIII spectrometer [5]. The two data sets agree well in the region of overlap. WASA has collected clean $pd \to {}^3\mathrm{He}\,\eta$, $\eta \to \gamma\gamma$ samples at 1450 and 1360 MeV. In addition, we analyzed the $pd \to {}^3\mathrm{He}\,\eta$ reaction *via* the $\eta \to \pi^0\pi^+\pi^-$ decay channel, which provided a cross check of the cut efficiency. There is a good agreement between the number of η mesons in the 2γ and 3π samples [28]. This shows that the effects of the cuts are well understood and that the yield of the events coming from outside the target is about the same in the $pd \to {}^3\mathrm{He}\,\eta$, $\eta \to \gamma\gamma$ case as when the cuts are optimized for selecting a ${}^3\mathrm{He}\,\pi^0\pi^+\pi^-$ final state (including $\pi^0\pi^+\pi^-$ production *via* η and ω).

The integrated luminosity L is calculated from

$$\frac{\Delta N}{\Delta\Omega} = \frac{d\sigma}{d\Omega} L, \tag{2}$$

where ΔN is the acceptance-corrected number of η candidates in the angular region $\Delta\Omega = 2\pi\,\Delta(\cos\theta^*_\eta)$, and $d\sigma/d\Omega$ is the differential cross section at this angle.

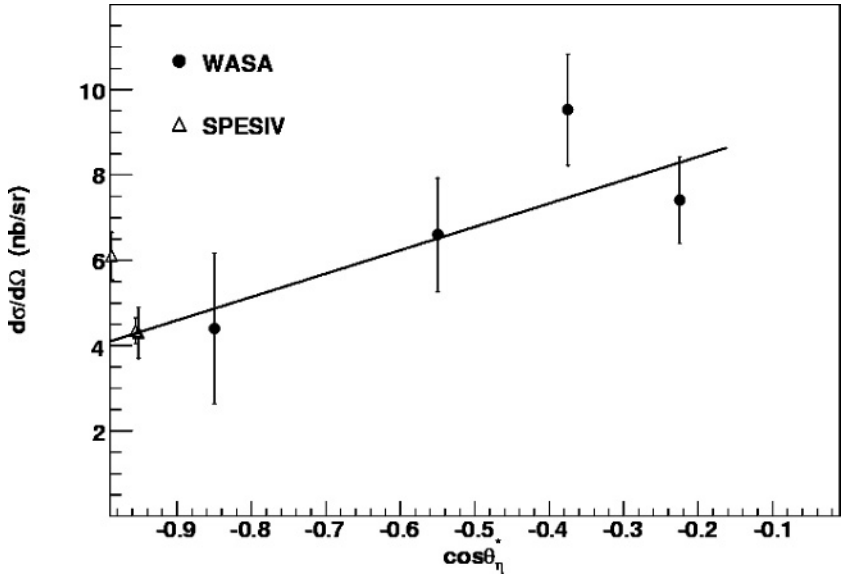

FIG. 5. Differential cross section data for the $pd \to {}^3\mathrm{He}\,\eta$ reaction used for the evaluation of the luminosity at 1360 MeV. The unfilled triangles are data from SPESIV [27] taken at $T_p = 1350$ MeV; the point at $\cos\theta^*_\eta = -0.96$ is used for normalization. The filled circles are WASA data taken at 1360 MeV and the line is the result of a linear fit to these.

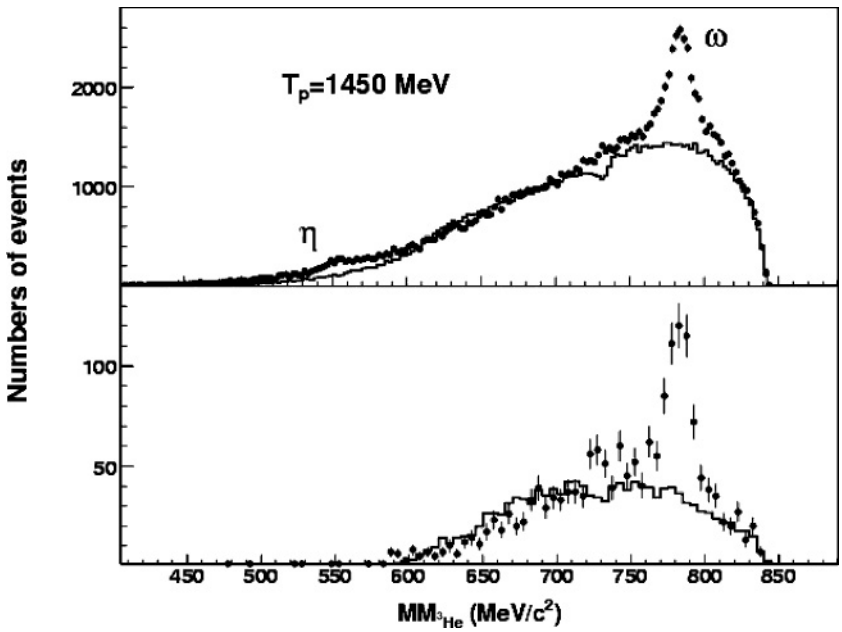

FIG. 6. Upper panel: Points are the distribution of missing mass of the ^{3}He, MM(^{3}He), for all events at 1450 MeV fulfilling the constraints optimized for $pd \to {}^3\mathrm{He}\,\omega, \omega \to \pi^0\pi^+\pi^-$ selection. The histogram shows the corresponding phase space simulations of the $pd \to {}^3\mathrm{He}\,\pi^0\pi^+\pi^-$ channel. Lower panel: MM(^{3}He) distribution for events fulfilling cuts optimized for selection of the $pd \to {}^3\mathrm{He}\,\omega, \omega \to \pi^0\gamma$ channel. The histogram is the phase space simulation of $pd \to {}^3\mathrm{He}\,\pi^0\pi^0$.

At 1450 MeV, there is a region $-0.99 < \cos\theta^*_\eta < -0.6$ where two WASA points overlap with a set of SPESIII and SPESIV points (see Fig. 4). In this region, the angular distribution is approximately isotropic. A fit to the combined SPESIII and SPESIV points to a constant gives a $\chi^2/\mathrm{ndf} = 1.8$. The resulting cross section, $d\sigma/d\Omega = 2.53 \pm 0.19$ nb/sr, where the statistical, systematic and normalization uncertainties of each point have been taken into account. A fit to the two WASA acceptance-corrected numbers of counts to a constant has an uncertainty of 9% and this contributes to the 12% overall uncertainty in the resultant luminosity.

The poorer $pd \to {}^3\mathrm{He}\,\eta$ database at 1360 MeV makes the situation more difficult at this energy and we have to rely on the few SPESIV points taken at $T_p = 1350$ MeV in the near-backward region [27]. At 1250 MeV and lower, this data set extends slightly further in angle and from this it is clear that, in addition to the very sharp backward peak, the angular distributions show a minimum for $\cos\theta^*_\eta \approx -0.96$ before rising less steeply at more forward angles. Though the four WASA points in the backward hemisphere shown in Fig. 5 are consistent with such a small rise, they do not overlap with the SPESIV data so that a linear fit has been made to extrapolate to the average of the two points in the $\cos\theta^*_\eta = -0.96$ region. It could be checked from the SPESIV data at 1450 MeV that the energy dependence in this region is negligible compared to a total normalization uncertainty of 29%, of which 27% arises from that in the linear extrapolation.

IV. RESULTS

A. $T_p = 1450$ MeV

The ω mesons are identified from the peak in the ^{3}He missing-mass distribution. The number of ω events is extracted by subtracting the background in two ways. The first is by fitting the background to a phase space Monte Carlo simulation of $pd \to {}^3\mathrm{He}\,\pi^0\pi^+\pi^-$ data. The second is by fitting the data as a Gaussian peak sitting on a polynomial background. The number of background events can then be estimated by integrating the polynomial. The central value and the width of the Gaussian peak obtained in the fit provide a quality control.

The difference in the number of ω events extracted by subtracting the background in these two ways gives the largest contribution to the systematic uncertainty. Applying the constraints defined in Sec. III B 1 gives a sample with a ^{3}He missing mass distribution shown in Fig. 6. After subtracting the background, we are left with 9900 ± 700 candidates for the $\omega \to \pi^0\pi^+\pi^-$ channel.

To verify that the systematics are under control, we made a cross-check using the $\omega \to \pi^0\gamma$ channel. On the basis of the evaluated acceptances and the known branching ratios, both summarized in Table I, we expect 520 ± 40 events from $\omega \to \pi^0\gamma$ in the sample. Selecting the events according to method described in Sec. III B 2 we get a number of 420 ± 50, which is fairly consistent.

The good match between the background continuum and the simulated $pd \to {}^3\mathrm{He}\,\pi^0\pi^+\pi^-$ in Fig. 6, the good agreement between the ω width in Monte Carlo and data, and the consistency between the results for the 3π and $\pi^0\gamma$ channels gives us confidence that the contribution from background not

TABLE I. Summary of the numbers of ω candidates found at different energies for the two decay channels.

Channel	T_p (MeV)	Acceptance (%)	BR (%) (%)	Number of candidates
$\omega \to \pi^+\pi^-\pi^0$	1450	35	89.1	9900 ± 700
$\omega \to \pi^0\gamma$	1450	19	8.7	420 ± 50
$\omega \to \pi^+\pi^-\pi^0$	1360	34	89.1	1800 ± 200
$\omega \to \pi^0\gamma$	1360	18	8.7	80 ± 20

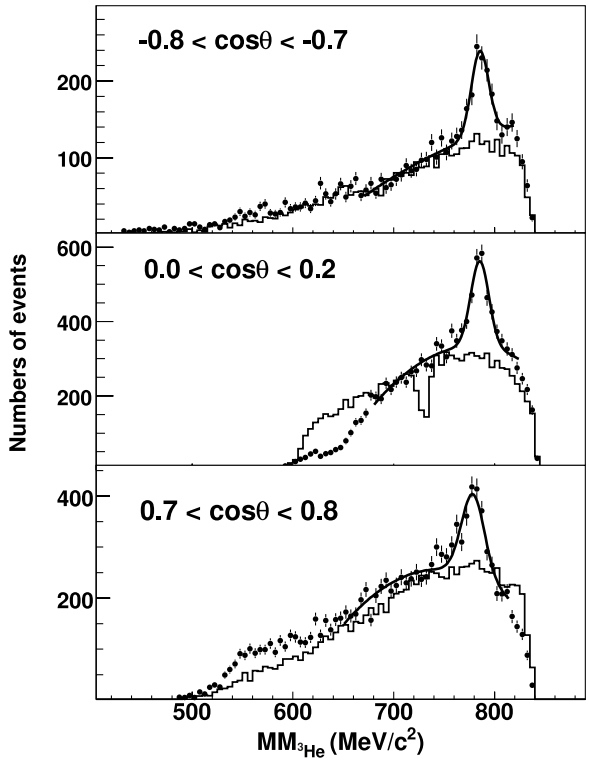

FIG. 7. Data taken in three angular regions at 1450 MeV, with cuts optimized for the $pd \to {}^3\mathrm{He}\,\omega$, $\omega \to \pi^0\pi^+\pi^-$ selection. Phase space simulations of $pd \to {}^3\mathrm{He}\,\pi^0\pi^+\pi^-$ production are also shown, as well as a fitted Gaussian peak on a polynomial background.

coming from reproducible physical reactions may be safely neglected.

In order to extract the differential cross section for the 3π sample, we divided the data into $\cos\theta^*_\omega$ bins and plotted separate ^{3}He missing-mass distributions, some examples of which are shown in Fig. 7. The number of ω events was then obtained by subtracting the background, which was estimated in the two ways described for the total sample. In some angular regions, the phase space simulated $\pi^0\pi^+\pi^-$ data did not follow perfectly the shape of the background. One then had to rely on the polynomial fit. The systematic uncertainty from background subtraction varies between 5% and 20%. Adding the ω candidates in each bin gives 9090, which is in good agreement with the value quoted in Table I. The numbers were corrected for acceptances that were derived from the phase space Monte Carlo simulations. Since the angular distribution is highly anisotropic, a fitted second degree polynomial was used as input. This reduced the total acceptance from 35% to 33%, though the effect for individual bins was negligible. This shows that the model dependence of the acceptance on angle is very weak. Finally we converted the numbers of ω mesons to cross sections by using the integrated luminosity discussed in Sec. III D.

The resulting $pd \to {}^3\mathrm{He}\,\omega$ angular distribution is shown in Fig. 8 along with the values obtained at SPESIII [5]. The two data sets agree in the backward direction, which lends confidence to our normalization procedure. However, although the WASA data do show a slight increase toward the forward direction, the sharp peak observed in Ref. [5] is not confirmed.

Fitting the angular distribution with Legendre polynomials results in an integrated cross section of $\sigma_{\mathrm{tot}} = 83.6 \pm 1.5 \pm 2.2$ nb, where the first uncertainty is statistical and the second systematic. In addition, however, there is an uncertainty of 12% that comes from the luminosity determination.

B. $T_p = 1360$ MeV

The analysis is more difficult at 1360 MeV than at the higher energy. The finite ω width ($\Gamma = 8.44$ MeV/c^2) leads to an asymmetric peak close to threshold since the high mass tail of the ω meson is then partially suppressed. Secondly, the background subtraction is more difficult since the multipion continuum ends under the ω peak (see Fig. 9). Thirdly, the signal-to-background ratio is small. To add to these difficulties,

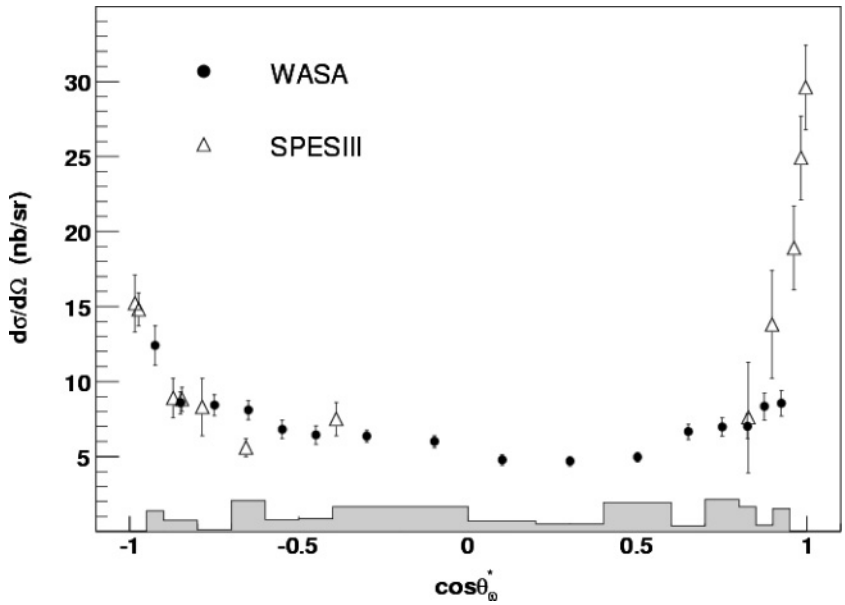

FIG. 8. $pd \to {}^3\mathrm{He}\,\omega$ differential cross section at 1450 MeV. The error bars on the WASA data (filled circles) show the statistical uncertainties while the grey histogram shows the systematical uncertainties due to background subtraction and acceptance correction. In addition there is an overall normalization uncertainty of 12%. The SPESIII results [5] are shown by the open triangles. The SPESIII error bars include statistical and systematical uncertainties and these data have an additional overall normalisation uncertainty of 20%.

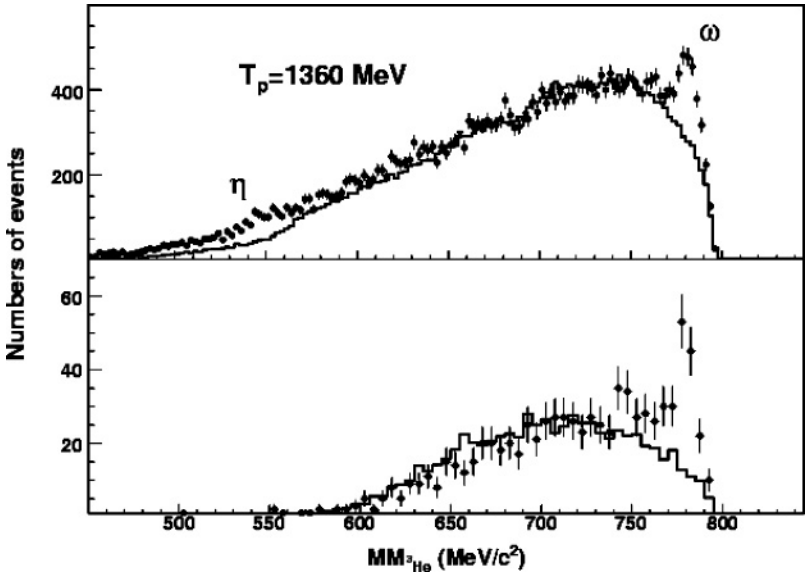

FIG. 9. MM(^{3}He) data at 1360 MeV for both the 3π and $\pi^0\gamma$ selection with experiment and simulation, as described for the 1450 MeV data of Fig. 6.

fewer data were taken at 1360 MeV than at 1450 MeV due to beam-time constraints. Higher systematic and statistical uncertainties are therefore to be expected at this energy.

Selecting data according to the methodology of Sec. III B 1 gives the data sample shown in the upper panel of Fig. 9 which, after background subtraction, leaves 1800 ± 200 ω events. Using the information given in Table I, we then estimate the number of $\omega \to \pi^0\gamma$ events should be 90 ± 10. This is to be compared to 80 ± 20 events obtained by subtracting the background in the lower panel of Fig. 9. The numbers from the two decay channels are thus quite consistent.

The extraction of the angular distribution was carried out in the same way as at 1450 MeV. The sum of the events in each angular bin (1600) agrees well with the 1800 found from Fig. 9. The angular distribution shown in Fig. 10 is consistent with isotropy and, within the total uncertainties, agrees with the point at 1360 MeV obtained by interpolating SPESIV results [6].

It was suggested in Ref. [6] that rescattering of decay pions off the ^{3}He nucleus might explain the observed threshold dip in the production amplitude. Their Monte Carlo simulations suggested that this would lead to a difference in the measured cross sections for the $\omega \to \pi^0\pi^+\pi^-$ and $\omega \to \pi^0\gamma$ modes of around 10% at 1360 MeV. Unfortunately, the uncertainties in the number of ω events from the two different channels obtained in the present experiment are too large to test this prediction.

Apart from the two points at $\cos\theta^*_\omega = -0.7$ and -0.55 in Fig. 10, which have especially large systematic as well as statistical uncertainties, the angular distribution is fairly flat and is in good agreement with the SPESIV point [6]. Excluding these points from a linear fit, the total cross section is

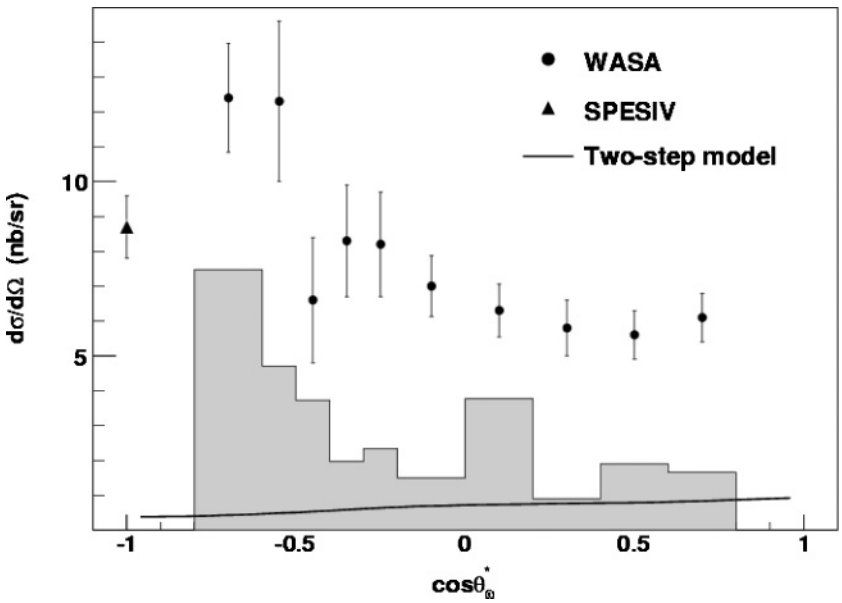

FIG. 10. Angular distributions for the $pd \to {}^3$He ω reaction at 1360 MeV, as described in Fig. 8 for the 1450 MeV results. In addition to the systematic uncertainties shown by the grey histogram, there is an uncertainty from normalization of 29%. The triangle shows the differential cross section obtained by interpolating the SPESIV data [6]. The error bar of the SPESIV point include the statistical and systematical uncertainties. The solid line represents the results of the model calculations described in Sec. V.

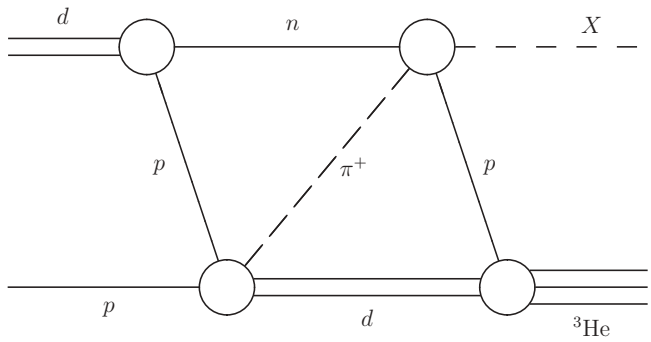

FIG. 11. Two-step model for the $pd \to {}^3\mathrm{He}\,X$ reaction where a virtual pion beam, created through $pp \to d\pi^+$, produces the observed meson X through a second $\pi^+ n \to pX$ reaction. There is a similar graph with a neutral intermediate pion.

determined to be $\sigma_{\mathrm{tot}} = 84.6 \pm 4.0 \pm 4.8$ nb. To this must be added the luminosity uncertainty of 29%.

V. MODEL CALCULATIONS

The minimum momentum transfer for the $pd \to {}^3\mathrm{He}\,\omega$ reaction at 1360 MeV is ~1110 MeV/c and this only drops to ~935 MeV/c at 1450 MeV. A direct production mechanism with such a large momentum transfer is expected to give vanishingly small cross sections. In order to share this large momentum between the nucleons, Kilian and Nann [29] suggested a two-step model, where a virtual pion beam is produced *via* a $pp \to d\pi^+$ reaction on the target proton, followed by the production of the observed meson X through the $\pi^+ n \to pX$ reaction on the target neutron, as illustrated in Fig. 11. There is an analogous contribution with an intermediate π^0.

The quantum-mechanical implementation of Fig. 11 describes well the total cross section for the production of the η-meson in pd collisions near-threshold [9,11,14]. The η angular distributions have been measured at several excess energies above about 20 MeV [30]. Although it had been claimed their shapes could be reproduced in a simplified two-step model [15], the most realistic implementation of this approach [12] fails to reproduce the data.

Theoretical studies of the $pd \to {}^3\mathrm{He}\,\omega$ cross section using a two-step model have been undertaken only close to threshold [10,14] and these underestimate the experimental data [6]. No predictions have yet been made for the ω angular distribution.

Following closely the implementation of the two-step approach described in Ref. [11], we evaluate the $\pi N \to \omega N$ subprocess using the Giessen model [31]. This is an effective Lagrangian approach that takes seven coupled channels in account, viz., γN, πN, $2\pi N$, ηN, ωN, $K\Lambda$, and $K\Sigma$, for the simultaneous analysis of all the data up to 2 GeV in terms of 11 isospin-$\frac{1}{2}$ resonances. It was shown in Ref. [31] that s-waves alone were insufficient to describe the $\pi N \to \omega N$ data even in the very near-threshold region. The full data set required partial waves up to $\ell = 3$ and their full amplitude analysis has been used as the basis for the construction of the $\pi N \to \omega N t$-matrix that is the required input for the $pd \to {}^3\mathrm{He}\,\omega$ estimation. The $pp \to d\pi^+$ input was taken from the parametrized t-matrix of the SAID group [32].

The results of the calculations performed in the plane wave approach to the two-step model, are shown in Figs. 10 and 12 at beam energies of 1360 MeV and 1450 MeV, respectively, along with the available data. Although the 1450 MeV predictions are reasonably close to the data in the central region, the shape is quite different to that of the experiment, giving forward and backward dips rather than peaks. There are therefore disagreements of up to an order of magnitude at the extreme angles. On the other hand, at 1360 MeV the two-step model predicts a fairly flat distribution with only a slight forward enhancement. However, it underestimates the cross section by a factor of about five in the forward region and by even more in the backward direction, which is a similar discrepancy to that reported in Ref. [14].

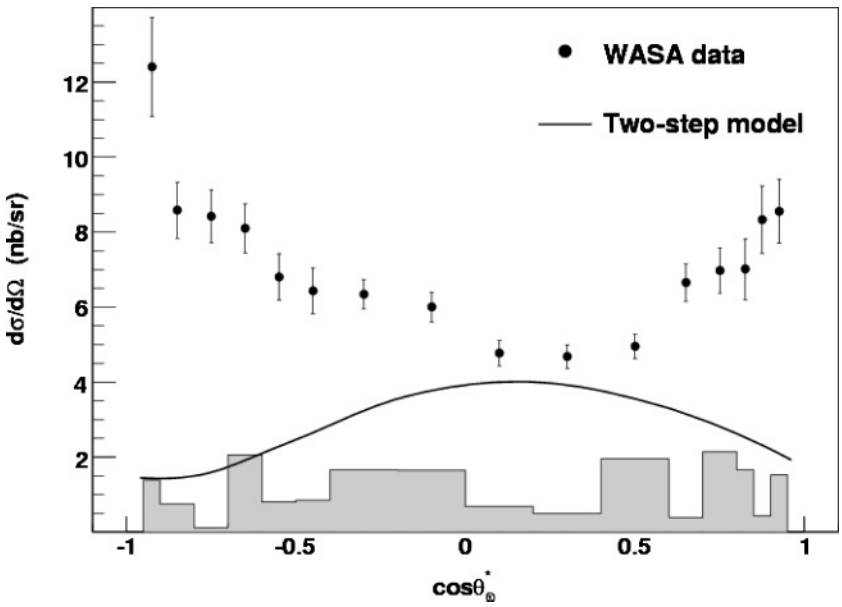

FIG. 12. Comparison of the WASA data on the $pd \to {}^3\mathrm{He}\,\omega$ reaction at 1450 MeV (filled circles) with calculations based upon a two-step approach (solid line). The meaning of the error bars and histogram is as in Fig. 8.

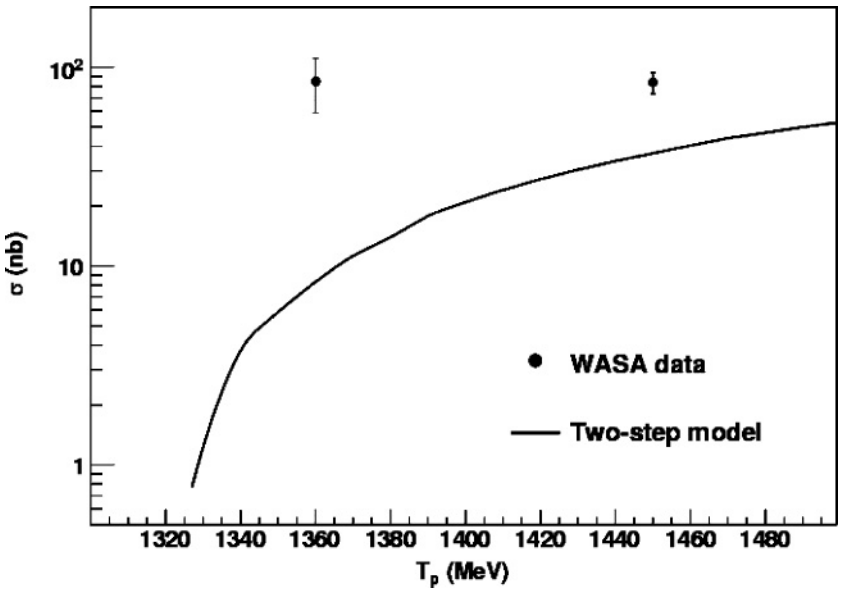

FIG. 13. The total cross section of $pd \rightarrow {}^3\mathrm{He}\,\omega$ reaction as a function of the beam kinetic energy. The filled circles are the two WASA points, where the error bars include the normalization uncertainties. The solid line shows the estimation within the two-step model presented in this work.

It should be stressed that the $pd \rightarrow {}^3\mathrm{He}\,\omega$ angular distribution is predicted to be anisotropic at 1360 MeV even if only s-wave are retained for the $\pi N \rightarrow \omega N$ vertex. This anisotropy persists in calculations carried out even closer to the threshold. It is perhaps interesting to note in this respect that experimental data on the $pd \rightarrow {}^3\mathrm{He}\,\eta$ reaction very near threshold show significant anisotropy [33].

We compare in Fig. 13 the total cross section calculated using the two-step model with the WASA data. Since this theoretical approach underestimates the differential cross sections, it also underpredicts the total cross sections.

Why does the two-step model fail for ω production? If the intermediate pion is taken on-shell, as in the Kilian and Nann classical model [29], the relative velocities of the deuteron from the $pp \rightarrow d\pi^+$ and the proton from the $\pi^+ n \rightarrow p\,\omega$ subprocesses are very large at the extreme angles at 1450 MeV. In contrast, at 1360 MeV, the change in the velocity matching over the full angular region is much less. The cross sections calculated using the two-step model at 1360 MeV thus describe the behavior of the experimental angular distribution but not its magnitude.

The poor velocity matching implies that the intermediate pion is a long way off its mass shell for both beam energies, unlike the case of the $pd \rightarrow {}^3\mathrm{He}\,\eta$ reaction at threshold. The predictions might be improved by using off-shell t-matrices for both $pp \rightarrow d\pi^+$ and $\pi^+ n \rightarrow p\,\omega$. However, it is clear that to reproduce the data at the extreme angles at 1450 MeV requires contributions from other diagram(s) since poor velocity matching is a kinematical effect that depends only upon the assumption of an intermediate pion. A similar conclusion might be drawn from the failure of the same model to describe well the $pd \rightarrow {}^3\mathrm{He}\,\eta$ angular distributions away from threshold [12].

VI. CONCLUSIONS

The differential cross section for the $pd \rightarrow {}^3\mathrm{He}\,\omega$ reaction has been measured over the full angular range at 1450 MeV. The data show clear anisotropy, with strong rises in both the backward and forward directions. For the backward-going ω the agreement with SPESIII data [5] is good, but the sharp forward peaking claimed at SPESIII is not confirmed by our data. The two-step model fails to describe the angular distribution, giving a convex rather than the concave shape found in our data.

The angular distribution at 1360 MeV is consistent with isotropy and, within the experimental uncertainties, the differential cross section for the backward-going ω agrees with the SPESIV point at $\cos\theta^*_\omega = -1$ [6]. If the assumptions in Refs. [7,8] that the SPESIV data are incorrectly interpreted are right, their point shown in Fig. 10 would be higher and the agreement with our data would become worse.

The large angular coverage of the WASA detector allowed values of the total cross sections at both energies to be extracted for the first time. At 1450 MeV we find $\sigma_{\mathrm{tot}} = 83.6 \pm 1.5 \pm 2.2$ nb, with an additional uncertainty from the normalization of 12%. The corresponding number at 1360 MeV is $\sigma_{\mathrm{tot}} = 84.6 \pm 4.0 \pm 4.8$ nb, where the additional normalization uncertainty is 29%.

The two-step model underestimates the total cross section data by a factor of about two at 1450 MeV and by a factor of ten at 1360 MeV. This is probably due to the velocity matching between the proton and deuteron produced in the two subprocesses being poor for some ω angles. Further theoretical work is therefore needed to describe both ω and η production in pd collisions.

ACKNOWLEDGMENTS

We wish to thank the personnel at the The Svedberg Laboratory for their support during the course of the experiment. We are grateful to Y. le Bornec for providing us with information regarding Ref. [5] and also V. Shklyar for supplying the t-matrix element of the Giessen model described in Ref. [31]. This work was supported by the European Community under the "Structuring the Research Area" Specific Program

Research Infrastructures Action (Hadron Physics, contract no. RII-cT-204-506078) by the Swedish Research Council, and BMBF (06TU201). K.P.K. wishes to thank the Fundação para a Ciência e a Tecnologia of the Ministério da Ciência, Tecnologia e Ensino Superior of Portugal for financial support under Contract No. SFRH/BPD/40309/2007.

[1] D. M. Binnie *et al.*, Phys. Rev. D **8**, 2789 (1973).
[2] J. Keyne *et al.*, Phys. Rev. D **14**, 28 (1976).
[3] H. Karami *et al.*, Nucl. Phys. **B154**, 503 (1979).
[4] F. Plouin, in *Production and Decay of Light Mesons*, edited by P. Fleury (World Scientific, Singapore, 1988), p. 114.
[5] T. Kirchner, Ph.D. thesis, IPN Orsay, France (1993).
[6] R. Wurzinger *et al.*, Phys. Rev. C **51**, R443 (1995).
[7] C. Hanhart and A. Kudryavtsev, Eur. Phys. J. A **6**, 325 (1999).
[8] C. Hanhart, A. Sibirtsev, and J. Speth, arXiv:hep-ph/0107245 (2001).
[9] G. Fäldt and C. Wilkin, Nucl. Phys. **A587**, 769 (1995).
[10] G. Fäldt and C. Wilkin, Phys. Lett. **B354**, 20 (1995).
[11] K. P. Khemchandani, N. G. Kelkar, and B. K. Jain, Nucl. Phys. **A708**, 312 (2002).
[12] K. P. Khemchandani, N. G. Kelkar, and B. K. Jain, Phys. Rev. C **68**, 064610 (2003).
[13] N. J. Upadhyay, K. P. Khemchandani, B. K. Jain, and N. G. Kelkar, Phys. Rev. C **75**, 054002 (2007).
[14] L. A. Kondratyuk and Yu. N Uzikov, Acta Phys. Pol. B **27**, 2977 (1996).
[15] M. Stenmark, Phys. Rev. C **67**, 034906 (2003).
[16] U. Tengblad, G. Fäldt, and C. Wilkin, Eur. Phys. J. A **25**, 267 (2005).
[17] K. Schönning *et al.*, Phys. Lett. **B668**, 258 (2008).
[18] F. Bellemann *et al.*, Phys. Rev. C **75**, 015204 (2007).
[19] Chr. Bargholtz *et al.*, Nucl. Instrum. Methods Phys. Res. A **594**, 339 (2008).
[20] C. Ekström *et al.*, Phys. Scr. **T99**, 169 (2002).
[21] Ö. Nordhage, Ph.D. thesis, Uppsala University, Sweden (2006).
[22] K. Schönning *et al.*, Acta Physica Slovaca **56**, 299 (2005).
[23] J. B. Birks, Proc. Phys. Soc. A **64**, 874 (1951).
[24] J. Złomaczuk, On Particle Identification in the WASA@COSY Forward Detector (2005), www.tsl.uu.se/jozef/docs/files/ParticleIdentification.pdf.
[25] Ö. Nordhage *et al.*, Nucl. Instrum. Methods Phys. A **569**, 701 (2006).
[26] Chr. Bargholtz *et al.*, Nucl. Instrum. Methods Phys. A **594**, 339 (2008).
[27] P. Berthet *et al.*, Nucl. Phys. **A443**, 589 (1985).
[28] K. Schönning, Ph.D. thesis, Uppsala University, Sweden (2009).
[29] K. Kilian and H. Nann, AIP Conf. Proc. **221**, 185 (1990).
[30] R. Bilger *et al.*, Phys. Rev. C **65**, 044608 (2002).
[31] V. Shklyar, H. Lenske, U. Mosel, and G. Penner, Phys. Rev. C **71**, 055206 (2005).
[32] R. A. Arndt, I. I. Strakovsky, R. L. Workman, and D. V. Bugg, Phys. Rev. C **48**, 1926 (1993).
[33] T. Mersmann *et al.*, Phys. Rev. Lett. **98**, 242301 (2007); J. Smyrski *et al.*, Phys. Lett. **B649**, 258 (2007).